FULL PAPER

Polymer Photovoltaic Cells Based on Solution-Processable Graphene and P3HT

By *Qian Liu, Zunfeng Liu, Xiaoyan Zhang, Liying Yang, Nan Zhang, Guiling Pan, Shougen Yin,* Yongsheng Chen,** and *Jun Wei*

A soluble graphene, which has a one-atom thickness and a two-dimensional structure, is blended with poly(3-hexylthiophene) (P3HT) and used as the active layer in bulk heterojunction (BHJ) polymer photovoltaic cells. Adding graphene to the P3HT induces a great quenching of the photoluminescence of the P3HT, indicating a strong electron/energy transfer from the P3HT to the graphene. In the photovoltaic devices with an ITO/PEDOT:PSS/P3HT:graphene/LiF/Al structure, the device efficiency increases first and then decreases with the increase in the graphene content. The device containing only 10 wt % of graphene shows the best performance with a power conversion efficiency of 1.1%, an open-circuit voltage of 0.72 V, a short-circuit current density of 4.0 mA cm^{-2}, and a fill factor of 0.38 under simulated AM1.5G conditions at 100 mW cm^{-2} after an annealing treatment at 160 °C for 10 min. The annealing treatment at the appropriate temperature (160 °C, for example) greatly improves the device performance; however, an annealing at overgenerous conditions such as at 210 °C results in a decrease in the device efficiency (0.57%). The morphology investigation shows that better performance can be obtained with a moderate content of graphene, which keeps good dispersion and interconnection. The functionalized graphene, which is cheap, easily prepared, stable, and inert against the ambient conditions, is expected to be a competitive candidate for the acceptor material in organic photovoltaic applications.

1. Introduction

In the past two decades, an ever increasing interest has been directed towards organic photovoltaic materials with the potential of providing low-cost alternatives to conventional inorganic solar cells because organic materials and solution-based fabrication procedures could reduce the power-consumption cost substantially, helping to drive a rapid expansion in the implementation of photovoltaic technology.[1] Solution processing, such as screen printing, doctor blading, inkjet printing, and spray deposition, provides an attractive route for achieving low-cost, large-area photovoltaic devices.[2] Conjugated polymers are excellent candidates for use in low-cost electronics and photovoltaic cells because of the simple, low-cost manufacturing of large-area, thin semiconductor films directly from solution. Additional advantages include the compatibility with flexible substrates and the low fabrication temperature, which allow devices to be fabricated on plastic substrates for flexible devices.[3,4] With significant advances in the fundamental understanding of the basic operation mechanisms and great effort to optimize their performance, conjugated-polymer-based solar cells have reached power-conversion efficiencies of 5–6% in recent reports.[5–10]

The commonly accepted mechanism for the light-to-electricity conversion process is:[2,11,12] i) light absorption exciton generation; ii) exciton diffusion; iii) exciton dissociation and charge formation; and iv) charge transport and charge collection. The conjugated polymers have highly conjugated π-systems; upon photon absorption, an electron is excited from the highest occupied molecular orbital (HOMO) to the lowest unoccupied molecular orbital (LUMO) and a strongly bound electron-hole pair (exciton) is generated. In contrast to the traditional inorganic semiconductors where free electrons and holes are generated under solar illumination, an energetic driving force must exist to separate this coulombic bound electron-hole pair.[2,12,13] In conjugated polymers, the separation of the photoexcited electron-hole pair can be achieved by creating a heterojunction with an acceptor material, which has an electron affinity (EA) that is larger than that of the polymer, but still smaller than its ionization potential (IP). By means of the difference in EA and IP of the two materials, the heterojunction supplies the driving force for charge separation that is necessary to dissociate the tightly bound electron-hole pairs into separate charges. In addition, the acceptor material should have a relatively lower HOMO level than the conjugated polymer in order to energetically favor the photoexcited conjugated polymer to transfer an electron to the

[*] Prof. S. G. Yin, Dr. Q. Liu, Dr. L. Y. Yang, Dr. N. Zhang, Prof. J. Wei
Key Laboratory of Display Materials and Photoelectric Devices
Institute of Material Physics, Tianjin University of Technology
300384, Tianjin (China)
E-mail: sgyin@tjut.edu.cn
Prof. Y. S. Chen, Dr. Z. F. Liu, Dr. X. Y. Zhang, Dr. G. L. Pan
Key Laboratory for Functional Polymer Materials and
Centre for Nanoscale Science and Technology
Institute of Polymer Chemistry
College of Chemistry, Nankai University
300071, Tianjin (China)
E-mail: yschen99@nankai.edu.cn

DOI: 10.1002/adfm.200800954

acceptor material and retain the hole in the polymer valence band, which is the lowest available energy state for the hole.[14] The heterojunction can be arranged in a bilayer, planar heterojunction structure[15] or an intermixed, bulk heterojunction (BHJ) structure.[16,17] The efficiency of the planar heterojunction device is limited by the exciton diffusion length, which is the distance over which excitons travel before undergoing recombination, also called the exciton diffusion bottleneck.[12,18–20] Excitons formed at a location further from the heterojunction sites than the exciton diffusion length have a lower probability of being harvested. Therefore, the thickness of the active layer of this type of solar cell is very thin and the solar-irradiation energy cannot be effectively absorbed, ultimately limiting the cell efficiency. The exciton diffusion bottleneck can be effectively reduced or overcome by applying the BHJ structure, where all excitons are formed within the exciton diffusion length in an interpenetrating network of the donor and acceptor materials.[1] In recent years, various BHJ photovoltaic devices have been made by use of polymer composites,[17,21–24] polymers with dyes,[25–27] polymers with fullerenes,[2,9,16,28] and small-organic-molecule composites.[29–31] Regarding fullerenes and their derivatives with a high EA and high charge mobility compared with other molecular acceptors, researchers have focused on polymer/fullerene BHJ photovoltaic devices. In particular, the combination of poly(3-hexylthiophene), (P3HT) with [6,6]-phenyl-C_{61}-butyric acid methyl ester (PCBM) has attracted intense interest and the cell efficiency has reached 5–6%.[5–10]

The ultimate efficiency of such BHJ devices is limited, however, by inefficient hopping charge transport,[32] and electron transport is further hindered by the presence of structural traps in the form of dead ends, isolated domains, and incomplete pathways in the random percolation network formed by the phase-segregation process.[33] Therefore, the challenge here is to provide continuous pathways within each component and thus allow charges to be transported efficiently to the electrodes before recombination occurs. One way to overcome the charge-transport limitation is to replace the 0D fullerenes with 1D nanomaterials such as carbon nanotubes (CNTs)[34–39] and inorganic nanorods.[33,40–44] Besides the high EA and high electron mobility, their long 1D structure is expected to reduce the number of interparticle hops required for electron extraction, and also reduce the presence of structural traps, and can then favor charge transfer.[33,44] Hybrid photovoltaic cells based on inorganic nanorod acceptors have reached an efficiency as high as 2%,[41] with much room to be further improved by fine control of the hybrid active layer, such as by the dispersion of the inorganic nanorods in the organic conjugated polymers to prevent agglomeration, assembly of the nanorods to form highly ordered nanostructures, and synthetic roles to control the radius, length, crystallinity, and wettability of the nanorods.[40] Although CNTs have unique characteristics, such as high charge mobility, long π-π conjugation and large aspect ratio, the efficiency of photovoltaic cells based on the acceptor of CNTs is rather low, usually below 0.5%.[34–39] This is because of a number of factors that limit their technological application, such as impurities in the CNTs, insolubility of the CNTs in common solvents, their polydispersity in length and diameter and the mixture of metallic and semimetallic types of CNT.[45]

Besides 0D fullerenes and 1D CNTs, graphene is another allotrope of carbon that is one atom thick with a 2D structure, and has been experimentally demonstrated to be stable at ambient conditions.[46] Pristine graphene has an electron mobility of 10 000 $cm^2\ V^{-1}\ s^{-1}$ at room temperature and has a micrometer-size two-dimensional plane with a large π-π conjugation. Electrons in graphene obey a linear dispersion relation and behave like massless relativistic particles, resulting in the observation of a number of very-peculiar electronic properties, such as the quantum Hall effect,[47–51] an ambipolar electric-field effect,[46] and transport via relativistic Dirac fermions.[52,53] Based on its fundamental electronic properties, graphene has been used to fabricate a number of electronic devices such as field-effect transistors,[54–58] resonators,[59] and quantum dots.[60] Based on its high conductivity and transmittance, conducting films[54,61] and transparent anodes[62,63] have also been developed. Graphene exhibits a high EA, high electron mobility, and a large 2D plane structure with one-atom thickness. When mixed with conjugated polymers, it is expected to be a good candidate for the acceptor material because large donor/acceptor (D/A) interfaces for charge generation and a continuous pathway for electron transfer will be formed in the graphene component. In previous research, we used graphene as the acceptor material, blended with poly(3-hexylthiophene) (P3HT)[64] and poly(3-octylthiophene) (P3OT)[65] to form BHJ photovoltaic cells, and a power conversion efficiency over 1% was obtained at 100 mW cm^{-2}. In this paper, we present detailed research of the photovoltaic performance of P3HT:graphene-based BHJ photovoltaic devices with regard to the device-fabrication details, annealing treatment, and morphology.

2. Results and Discussion

2.1. Synthesis of Solution-Processable Functionalized Graphene

There have been several methods used to fabricate graphene used for electronic devices, such as micromechanical cleavage,[46] epitaxial growth,[66,67] and others.[68] The graphene prepared by these methods is on a very-small scale and is insoluble in common solvents: it is therefore hardly to be used in polymer-composite-based applications. As recent efforts on the successful preparation of graphene-based composites have greatly progressed, many electronic applications have been realized by combining the graphene and the matrix.[61,69,70] The successful preparation of graphene-polymer composites was initially reported by Stankovich et al.,[69] where they mechanically mixed the functionalized graphene with polystyrene, and the resulting composite rendered a high conductivity and a low percolation threshold. By the use of a similar method, a solution-processable functionalized graphene (SPFGraphene)/P3HT composite was prepared and used as the active layer in the photovoltaic devices in this study. The SPFGraphene was prepared by a two-step method: an oxidation step and then an organic functionalization step.[69] Firstly, using a modified Hummers method[71] as described elsewhere,[63] water-soluble, heavily oxygenated graphene oxide (GO) sheets was generated by introducing polar functional groups such as –COOH, –OH, as well as –C=O, –C–O–C–, and

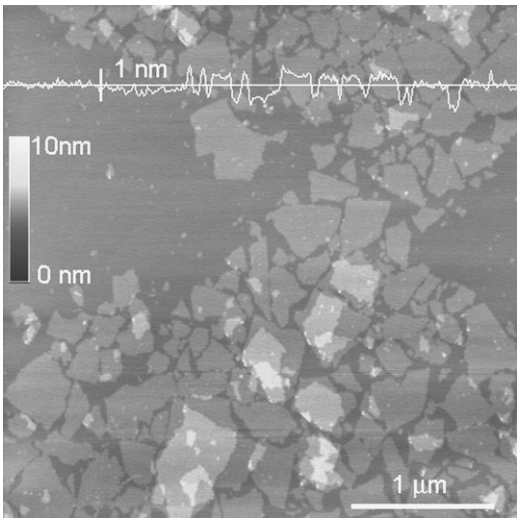

Figure 1. AFM image of the GO after the oxidation process, in tapping mode. The GO sample was prepared by spin coating (2 000 rpm, 30 s) a GO water solution (0.2 mg mL^{-1}) on a mica surface.

$-CH_2-$ into the graphene sheet.[72] The GO sheets can be readily dispersed in water with mild sonication, which contains mainly individual functionalized graphene sheets as the concentration deceases to some extent.[73] Figure 1 shows an atomic force microscopy (AFM) image of the GO. It can be seen that most of the graphene oxide sheets have a thickness in the range of 0.7–0.8 nm. In this strong oxidation process, the graphene sheets were cut into small pieces with a size of several hundred nanometers. From the fact that the thickness is uniformly distributed, and that sheets one half (or other smaller inverse-integer value) of the observed minimum thickness are never detected, it is believed that these typical GO sheets are fully exfoliated.[73] While the pristine, single-graphene sheet is flat with a van der Waals thickness of ~0.34 nm,[74] the graphene oxide sheets are thought to be thicker because of the presence of covalently bound oxygen and the displacement of the sp^3-hybridized carbon atoms on both surfaces of the original graphene plane, as indicated in the literature.[75,76]

Given the hydrophilic nature of the GO sheets, their application as fillers of organic polymer matrices in hydrophobic organic solvents is hindered. Therefore, for the second step, functionalization, a chemical functionalization process was carried out to change the surface properties of the GO using an organic isocyanate: phenyl isocyanate.[69,77] As a result, the isocyanate-derived graphene oxide (SPFGraphene) develops a hydrophobic nature and can be easily dissolved in organic solvents such as 1,2-dichlorobenzene (DCB). This means the graphene sheets become homogenously dispersed with organic materials, especially conjugated polymers in organic solvents used for photovoltaic applications. Using elemental analysis, the weight fractions of N, C, and H of the SPFGraphene were determined to be 4.89–4.95%, 60.28–60.32%, and 4.45–4.51%, respectively. Based on this, the functional group of $-NH-C_6H_5$ from the –OH and –COOH group was estimated to be 14 per 100 C atoms in the graphene sheets, consistent with that of previously reported phenyl isocyanated graphene;[77] a schematic representation of the chemical structure of SPFGraphene is shown in Figure 2a.

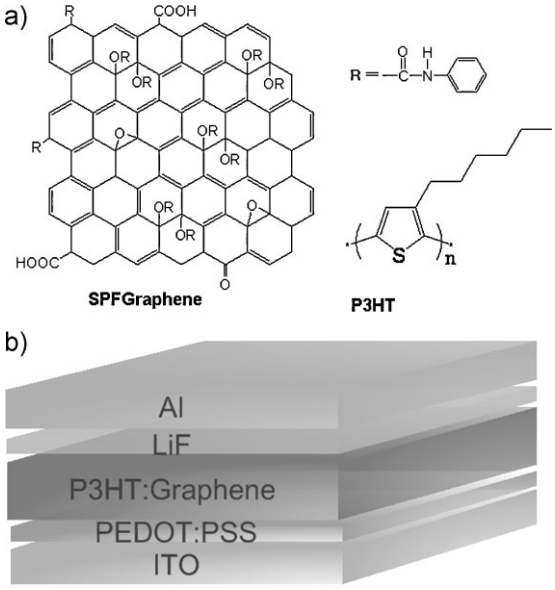

Figure 2. a) The schematic chemical structure of SPFGraphene and P3HT. b) Schematic structure of the devices with the P3HT/SPFGraphene thin film as the active layer; ITO (~17 Ω sq^{-1})/PEDOT:PSS (40 nm)/P3HT:SPFGraphene (100 nm)/LiF (1 nm)/Al (70 nm).

2.2. Spectroscopic Properties

The P3HT/SPFGraphene mixture solution was prepared by dissolving the P3HT and SPFGraphene in DCB, and was characterized by absorption spectroscopy. Figure 3 shows the normalized UV/visible/near-IR (NIR) absorption spectra of the P3HT/SPFGraphene (P3HT: 1 mg mL^{-1}, SPFGraphene content: 10 wt %) diluted solution in DCB, as well as a reference solution of P3HT (1 mg mL^{-1}) in DCB. The presence of P3HT in the solution is characterized by the absorption band between 350 to

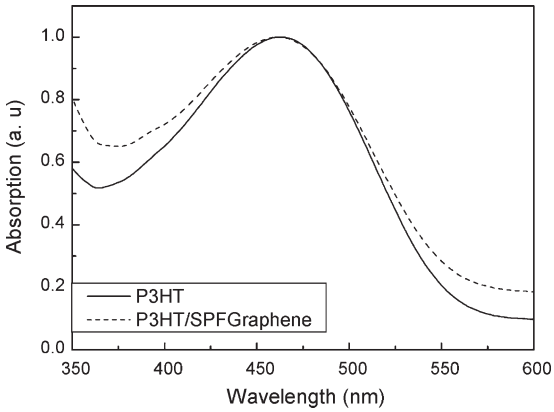

Figure 3. Normalized UV/vis/NIR absorption spectra of P3HT and P3HT/SPFGraphene (P3HT: 1 mg mL^{-1}, SPFGraphene content: 10 wt %) in 1,2-dichlorobenzene.

600 nm, with a peak at 450 nm. It can be seen that the P3HT/SPFGraphene mixture solution has almost the same absorption range and peak as that of the pure P3HT solution in the wavelength range from 350 to 600 nm, except that the absorption peak of the P3HT/SPFGraphene mixture solution is slightly broadened, and absorbs more strongly below 400 nm and above 550 nm. This should be caused by the absorption of SPFGraphene in the composite film. The absorption spectrum of the P3HT solution shows no significant change upon adding 10 wt % of SPFGraphene. This implies that in the P3HT/SPFGraphene mixture solution, no significant ground-state interactions take place between the two materials, and hence, no charge transfer occurs in the ground state, which is consistent with the literature.[38,78]

For BHJ photovoltaic cells, photoinduced charge transfer from the donor polymer to the acceptor is usually needed for the photocurrent generation. Photoluminescence (PL) in conjugated thiophenes is well known to arise from radiative recombination of polaron-exciton pairs into Franck–Condon (FC) states,[79,80] and the quenching of the PL of an appropriate donor polymer by a suitable acceptor gives an indication of an effective photoinduced charge transfer from the donor to the acceptor, as described by Sariciftci et al.[81] for composites of p-type conducting polymers and fullerene derivatives. Thus, the PL spectra of the P3HT/SPFGraphene (P3HT: 1 mg mL^{-1}, SPFGraphene content: 10 wt %) mixture solution in DCB and the P3HT (1 mg mL^{-1}) solution in DCB were investigated, as shown in Figure 4.

From Figure 4 it can be seen that the P3HT solution shows strong photoluminescence between 525 and 750 nm, with excitation at 422 nm, while the photoluminescence is remarkably reduced after the SPFGraphene was introduced, showing efficient charge/energy transfer along the P3HT/SPFGraphene interface. These results show that the excited fluorophore in the P3HT backbone was quenched by the electronic interactions at the P3HT/SPFGraphene interfaces. By referencing previous work with PCBM[82] and carbon nanotubes,[78] this efficient quenching of the PL emission shows that graphene is expected to be an effective electron-acceptor material for organic photovoltaic applications.

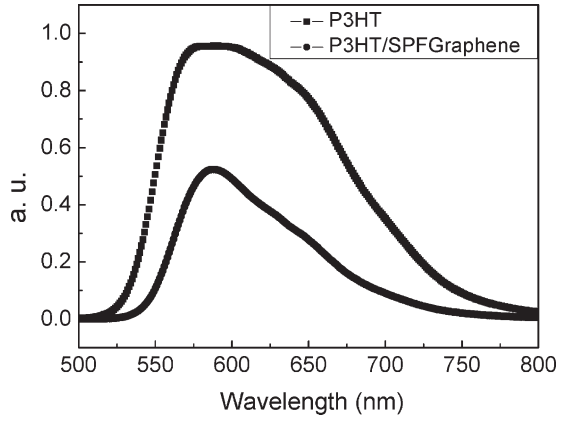

Figure 4. Photoluminescence spectra of P3HT/SPFGraphene (P3HT: 1 mg mL^{-1}, SPFGraphene content: 10 wt %) mixture solution in DCB and P3HT (1 mg mL^{-1}) solution in DCB at an excitation wavelength of 422 nm.

2.3. Photovoltaic Characterization

We fabricated photovoltaic devices using a common fabrication process. The active layer was prepared by spin-coating P3HT (15 mg mL^{-1})/SPFGraphene solutions in DCB (SPFGraphene contents: 0 wt %, 2.5 wt %, 5 wt %, 10 wt %, 15 wt %) onto indium tin oxide (ITO) glass substrates which were precoated with poly(ethylene dioxythiophene) doped with polystyrene sulfonic acid (PEDOT:PSS, a conducting polymer); then LiF and Al layers were vapor-deposited onto the active layer. The chemical structure of P3HT is shown in Figure 2a. A schematic representation of the P3HT/graphene-based solar cell is shown in Figure 2b; it has a structure of ITO (~17 Ω sq^{-1})/PEDOT:PSS (40 nm)/P3HT:SPFGraphene (100 nm)/LiF (1 nm)/Al (70 nm). The current–voltage (*J*–*V*) curves of the photovoltaic devices were determined using an AM1.5G standard operating with an illumination intensity of 100 mW cm^{-2}, as shown in Figure 5.

Figure 5a shows the logarithmic *J*–*V* curves of the photovoltaic devices based on P3HT and P3HT/SPFGraphene (SPFGraphene content: 10 wt %) in the dark and under illumination. It can be seen that there is no current response in the dark for the two photovoltaic devices: the high dark current under forward bias indicates a distinct diode behavior. Under illumination, the device based on pristine P3HT gives a power-conversion efficiency (η) of 0.005%, a short-circuit current density (J_{sc}) of 0.04 mA, an open-circuit voltage (V_{oc}) of 0.42 V, and a fill factor (*FF*) of 0.27; while the P3HT/SPFGraphene based one gives an $\eta = 0.15\%$, $J_{sc} = 0.46$ mA, $V_{oc} = 1.1$ V, and $FF = 0.30$. The overall performance of the P3HT/SPFGraphene based device is much higher than that of the control device based on pristine P3HT. Obviously, the improvement in the overall photovoltaic performance can be attributed to the addition of SPFGraphene, indicating that there is an obvious charge transfer from the P3HT donor to the SPFGraphene acceptor, as shown in Figure 5a. We then investigated the photovoltaic characteristics based on the P3HT/SPFGraphene composite containing different SPFGraphene contents (2.5 wt %, 5 wt %, 10 wt %, and 15 wt %), as shown in Figure 5b, and the performance details are listed in Table 1. The devices with SPFGraphene contents of 2.5 wt %, 5 wt %, 10 wt %, and 15 wt % show η values of 0.09%, 0.1%, 0.15%, and 0.13%, respectively. It can be seen that with an increase in the SPFGraphene content, the overall performance increases first, reaching a peak efficiency of 0.15% for the 10 wt % SPFGraphene content, and then decreases. The devices with the SPFGraphene content of 2.5 wt %, 5 wt %, 10 wt %, and 15 wt % show V_{oc} values of 0.84, 0.88, 1.1, and 0.72 V, J_{sc} values of 0.48, 0.36, 0.46, and 0.75 mA cm^{-2}, and *FF* values of 0.23, 0.28, 0.3, and 0.25 respectively. It can be seen that with the increase in the SPFGraphene content, the V_{oc} values increase first, and then decreases, varying in the range of 0.7–1.1 V, while the J_{sc} values show an increasing tendency. The device with an SPFGraphene content of 15 wt % shows the highest J_{sc} value and the lowest V_{oc} value of the four samples. The *FF* values are relatively low, and with the increase in the SPFGraphene content, they increase first and then decrease. In general, the overall performances of the P3HT/SPFGraphene based photovoltaic devices are relatively low, the best cell efficiency being only 0.15%. After organic functionalization of the graphene sheet rendering it soluble, its large conjugated structure is highly destroyed. There are ~14

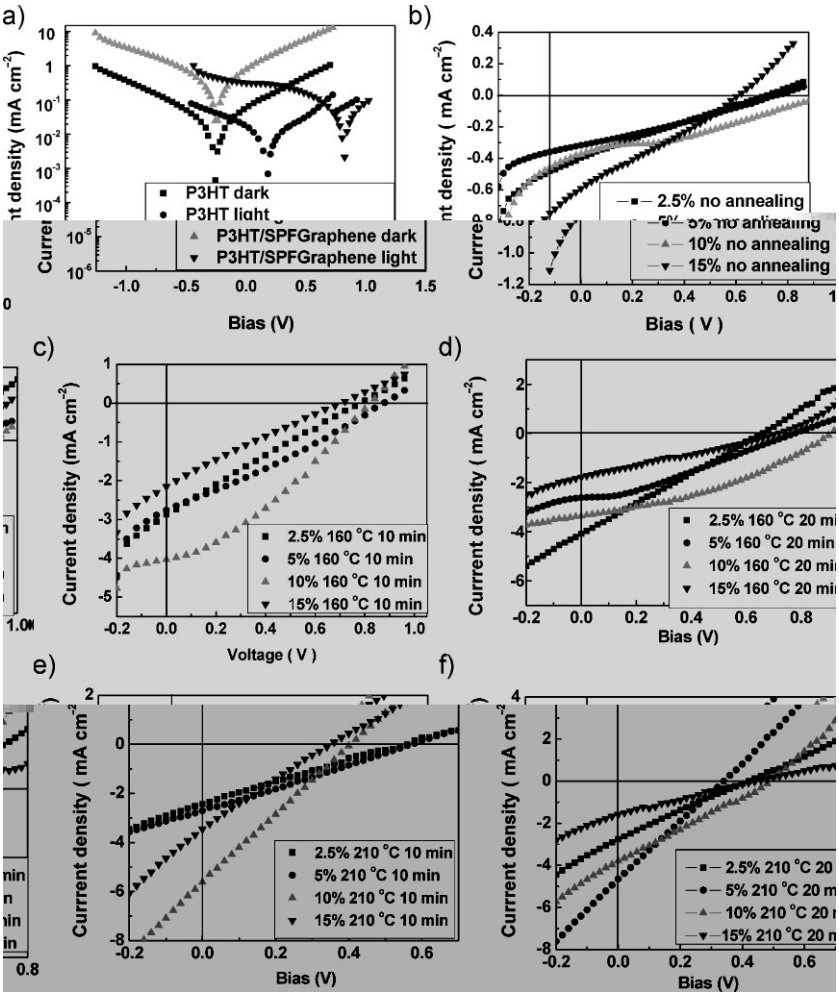

Figure 5. a) Logarithmic *J–V* characteristics of the photovoltaic devices based on P3HT and P3HT/SPFGraphene in the dark and under a simulated AM1.5G 100 mW illumination. b–f) *J–V* characteristics of the P3HT/SPFGraphene-based photovoltaic devices with different graphene contents (2.5 wt %, 5 wt %, 10 wt %, and 15 wt %) under a simulated AM1.5G 100 mW illumination without annealing, with annealing at 160 °C for 10 min, with annealing at 160 °C for 20 min, with annealing at 210 °C for 10 min and with annealing at 210 °C for 20 min, respectively.

–NH–C_6H_5 groups, from –OH and –COOH groups, per 100 C atoms in the graphene sheet, as well as –C=O, –C–O–C–, and –CH_2– groups in the graphene sheet. Therefore, the charge-transport mobility of the graphene sheets used in the above photovoltaic device must decrease dramatically and then the device performance will be inhibited by the charge transfer. Recent reports have shown that the common organic functional groups are unstable at high temperatures and can be removed from the graphene sheet by thermal reduction and that the conjugated structure of the graphene sheet can be partially recovered and the charge-transport ability can be increased greatly.[62,63] Therefore, we investigated the thermal properties of the SPFGraphene by using thermogravimetric analysis (TGA) and differential scanning calorimetry (DSC), the results of which are shown in Figure 6.

2.4. Annealing Treatment and Photovoltaic Performance

From the TGA curve in Figure 6 it can be seen that there is approximately 8% weight loss below 100 °C, which we see accompanies an endothermic process. This process can be attributed to the evaporation of small molecules, such as solvent molecules, remaining in the SPFGraphene. Then, the TGA curve shows a typical plateau from 100 °C to 150 °C, where we can only see a slow weight loss of ~2%. Following this plateau a greater weight loss of ~20% occurred from 150 to 250 °C, and in this temperature range an obvious exothermic peak at 189 °C can be observed in the DSC curve. The weight loss in this temperature range can be attributed to the removal of functional groups from the graphene sheets. By further increasing the temperature to 960 °C, the weight loss gets slower and slower and a plateau is formed again in the TG curve. Therefore, in order to remove the organic functional groups from the graphene sheet and recover the conjugated structure and conductivity of the graphene sheet, we carried out an annealing treatment of the devices after spin-coating of the active layer at different temperatures (160 and 210 °C) and time durations (10 min and 20 min). The photovoltaic performances of devices made from these materials are shown in Figure 5c–f.

Figure 5c shows the performance of the P3HT/SPFGraphene devices after an annealing treatment at 160 °C for 10 min, and the detailed photovoltaic characteristics are also listed in Table 1. It can be seen that a great improvement in the photovoltaic performances for all the devices was achieved after annealing. The η values are 0.55%, 0.69%, 1.1%, and 0.35% for the devices with SPFGraphene contents of 2.5 wt %, 5 wt %, 10 wt %, and 15 wt % respectively. After the annealing treatment, the dependence of the cell efficiency upon the SPFGraphene content is similar as that without an annealing treatment. The cell performance increases first with the increase in SPFGraphene content, achieving a peak value of 1.1% at an SPFGraphene content of 10 wt %, and then decreases. The V_{oc} values for the devices with SPFGraphene contents of 2.5 wt %, 5 wt %, 10 wt %, and 15 wt % are 0.78, 0.86, 0.72, and 0.78 respectively, in the range of 0.7–0.9 V, slightly different from those of the unannealed ones. A very interesting observation is that the J_{sc} values increase by almost one order of magnitude and the fill factor also increases. After the annealing treatment, the J_{sc} values of the four devices are 2.9, 2.7, 4.0, 2.1 mA cm^{-2}, and the *FF* values are 0.24, 0.3, 0.38, and 0.21, respectively. Obviously, the annealing process plays an important role in the improvement of the device performance. With the removal of the functional

Table 1. Performance details (V_{oc}, J_{sc}, *FF*, and η) of the P3HT/graphene-based photovoltaic devices without annealing and after annealing at 160 °C and 210 °C for 10 min and 20 min under a simulated AM1.5G 100 mW illumination.

Graphene content	Annealing temperature	Annealing time	V_{OC}	J_{SC}	*FF*	η
[wt %]	[°C]	[min]	[V]	[mA cm^{-2}]		[%]
0	–	–	0.42	0.04	0.27	0.005
2.5	–	–	0.84	0.48	0.23	0.09
5	–	–	0.88	0.36	0.28	0.10
10	–	–	1.10	0.46	0.30	0.15
15	–	–	0.72	0.75	0.25	0.13
2.5	160	10	0.78	2.9	0.24	0.54
5	160	10	0.86	2.7	0.30	0.69
10	160	10	0.72	4.0	0.38	1.10
15	160	10	0.78	2.1	0.21	0.35
2.5	160	20	0.66	4.1	0.25	0.68
5	160	20	0.78	2.6	0.31	0.63
10	160	20	0.88	3.3	0.39	1.10
15	160	20	0.72	1.8	0.27	0.35
2.5	210	10	0.56	2.4	0.25	0.33
5	210	10	0.58	2.7	0.26	0.40
10	210	10	0.40	5.6	0.25	0.57
15	210	10	0.36	3.5	0.23	0.29
2.5	210	20	0.42	2.8	0.23	0.27
5	210	20	0.34	4.7	0.24	0.39
10	210	20	0.48	3.8	0.26	0.47
15	210	20	0.44	1.6	0.26	0.18

groups and recovery of the π-conjugated areas, the conductivity of the graphene sheet and the charge carrier-transport mobility increase greatly.[62] In addition, the morphology change of P3HT can also be an import contribution to the improvement in the device performance.[28]

As can be seen in the TGA and DSC curves shown in Figure 6, the annealing treatment for a longer time and at a higher temperature will result in further removal of the functional groups from the graphene sheet, and then a more-sufficient recovery in the π-conjugated structure and in the charge-transport mobility. Therefore, we carried out the annealing treatment of the P3HT/SPFGraphene devices at 160 °C for 20 min, at 210 °C for 10 min, and at 210 °C for 20 min; the photovoltaic performances are shown in Figures 5d, 5e, and 5f, respectively, and are also listed in Table 1.

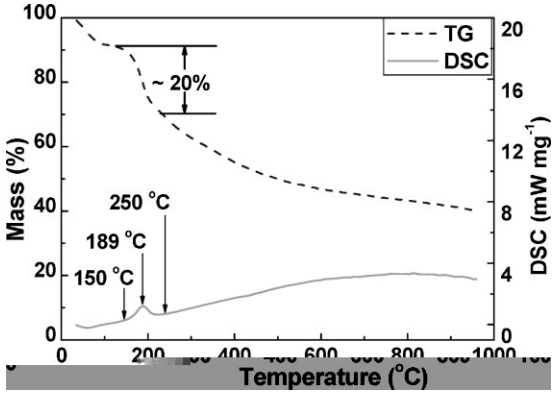

Figure 6. Thermogravimetric analysis (TGA) and differential scanning calorimetry (DSC) curve of the SPFGraphene in the temperature range from 35 to 960 °C at a heating rate of 5 °C min^{-1} under nitrogen flow.

Annealing of the devices with SPFGraphene contents of 2.5 wt %, 5 wt %, 10 wt %, and 15 wt % at 160 °C for 20 min gives η values of 0.68%, 0.63%, 1.1%, 0.35%, respectively. These show comparable absolute values and a similar dependence on the SPFGraphene content compared with the devices annealed at 160 °C for 10 min. The devices with the SPFGraphene contents of 2.5 wt %, 5 wt %, 10 wt %, and 15 wt % show V_{oc} values of 0.66, 0.78, 0.88, 0.72 V, J_{sc} values of 4.1, 2.6, 3.3, and 1.8 mA cm^{-2}, and *FF* values of 0.25, 0.31, 0.39, and 0.27, respectively. This shows that prolonging the annealing time at 160 °C has a slight influence on the device performance.

After annealing at 210 °C, the devices' performances decrease greatly compared with those annealed at 160 °C, including V_{oc}, J_{sc}, and η as shown in Table 1. The devices with SPFGraphene contents of 2.5 wt %, 5 wt %, 10 wt %, and 15 wt % annealed at 210 °C for 10 min show V_{oc} values of 0.56, 0.58, 0.4, and 0.36 V, J_{sc} values of 2.4, 2.7, 5.6, and 3.5 mA cm^{-2}, and η values of 0.33%, 0.40%, 0.57%, and 0.29%, respectively. The above four devices annealed at 210 °C for 20 min show V_{oc} values of 0.42, 0.34, 0.48, and 0.44 V, J_{sc} values of 2.8, 4.7, 3.8, and 1.6 mA cm^{-2}, and η values of 0.27%, 0.39%, 0.47, and 0.18% respectively. The η values show a similar dependence on the SPFGraphene content compared with the devices annealed at the other conditions, that is, with the increase in the SPFGraphene content: the η values increase at first, reaching a peak value at the SPFGraphene content of 10 wt % (0.57% and 0.47% for the devices annealed at 210 °C for 10 min and 20 min), and then decrease. No great changes can be observed in the *FF* values upon annealing the devices under different conditions: the *FF* values are in the range of 0.2–0.3. These results show a relatively high series

resistance for the devices, which may be caused by inefficient stacking of the graphene sheets in the P3HT matrix, as will be discussed in the following section about morphology analysis of the composite films. The V_{oc} value of the devices decreases to ~0.4–0.6 V after annealing at 210 °C for 10 min and further decreases to ~0.3–0.5 V when annealing for 20 min. The J_{sc} values of the devices are also lower, compared with those of the devices annealed at 160 °C. This indicates that annealing the devices under overgenerous conditions is deleterious to the device performance, especially in V_{oc}.

In order to evaluate the effect of the annealing conditions on the photovoltaic performance, V_{oc}, J_{sc}, *FF*, and η were plotted via the SPFGraphene content under different annealing conditions, as shown in Figure 7.

From Figure 7a, it can be seen that the devices without annealing show V_{oc} values in the range of ~0.7–1.1 V; the devices annealed at 160 °C shows V_{oc} values in the range of ~0.7–0.9 V, while upon annealing at 210 °C, the V_{oc} values decrease greatly to ~0.3–0.5 V. Different models have been proposed for the origin of the V_{oc}.[83,84] In a single, layered, organic photovoltaic cell, in which the active layer is composed of a pure conjugated polymer, the open circuit voltage, V_{oc}, is principally determined by the difference of the work functions between the two metal electrodes: the metal-insulator-metal (MIM) model.[84] In this model, the polymer is assumed to have a negligible amount of intrinsic charge carriers and can therefore be seen as an insulator. Hence, the upper limit of the V_{oc} can be calculated from an estimation of the difference between the work function of the two electrodes. As measured in our controlled ITO/P3HT/LiF/Al device, we get a V_{oc} value of 0.42 V, which matches the work-function difference (0.4 V) of the ITO (4.7 eV) and the Al cathode (4.3 eV) perfectly. However, the MIM model cannot be applied to solar cells with a BHJ structure, such as those based on polymer-fullerene composites. It has been found that the V_{oc} is highly dependent on the lowest unoccupied molecular orbital (LUMO) level of the acceptors,[85] suggesting that a Fermi level pinning between the negative electrode and the fullerene could be the origin of the Ohmic-like behavior of the fullerene-negative electrode contact.[83] Therefore, the upper limit of the V_{oc} can be determined by the difference of the fullerene LUMO and the polymer's highest occupied molecular orbital (HOMO) energy levels.[83,85] Similarly, a pinning mechanism between the negative electrode and the single-walled nanotubes (SWNTs) was also applied in the solar cells based on polymer-carbon nanotube composites, and V_{oc} is governed by the work function of carbon nanotube as well as the HOMO level of the conjugated polymer.[39] Thus, in our P3HT/graphene-based devices, such a pining mechanism may be applied to describe the origin of V_{oc} value. The calculated work function of pristine graphene is 4.42 eV[86] and the most-commonly reported work function of as-prepared graphene is around 4.5 eV.[87] Therefore, if the work-function value of the unfunctionalized graphene is used here, the upper limit of the V_{oc} may be determined by the difference of the work function of graphene (4.5 eV) and the HOMO level (5.2 eV) of P3HT,[88] and a V_{oc} of ~0.7 V is expected. This value is lower than that of both the P3HT/SPFGraphene devices without annealing (~0.7–1.1 V) and with annealing at 160 °C (~0.7–0.9 V). This may be caused by the following reasons: i) different from the pristine graphene sheet, the functionalized one is influenced by some functional groups and its large π-conjugated structure is partly isolated by them, which alters the work function of graphene sheet, more or less; ii) similar to the P3HT/SWNTs-based donor/acceptor system, strong π-π conjugation between the graphene and the P3HT may raise the Fermi level of the graphene.[36] Upon annealing at 210 °C, the V_{oc} values decrease greatly to ~0.3–0.5 V, much lower than ~0.7 V. This may also be caused by two possible reasons: i) the removal of the functional groups at 210 °C from the graphene sheet may alter its work function to a much-higher level, and then the difference between the work-function value of the functionalized graphene and the HOMO level of the P3HT decreases; ii) the electron-transport mobility in the graphene sheet after annealing at 210 °C may be recovered to reach a high value, resulting in low quasi-Fermi levels for electrons and holes and thus the V_{oc} value is reduced.[89]

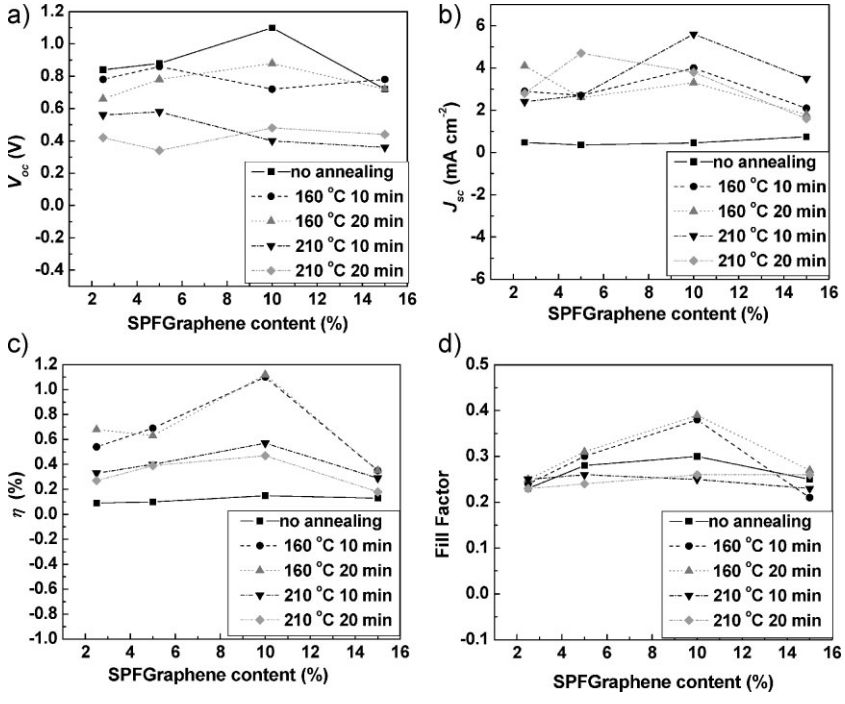

Figure 7. Dependence of V_{oc}, J_{sc}, η, and fill factor (*FF*) for the photovoltaic devices under different annealing conditions (without annealing, annealing at 160 °C for 10 min, annealing at 160 °C for 20 min, annealing at 210 °C for 10 min, and annealing at 210 °C for 20 min) on the SPFGraphene content in the P3HT/SPFGraphene composites.

It can also be seen from Figure 7b–d that the annealing treatment improves the device performance in terms of J_{sc}, η, and *FF* at 160 °C, while annealing at overgenerous conditions such as 210 °C results in a decrease of the device performance. These devices show similar performance dependence, in terms of

J_{sc}, η, and *FF*, on the SPFGraphene content upon annealing under different conditions, compared to the unannealed ones; that is to say, with the increase in the SPFGraphene content, the device performance increases first, reaching a peak value at an SPFGraphene content of 10 wt %, and then decreases.

2.5. Morphology Investigation

In order to help understand the dependence of the photovoltaic performance on the SPFGraphene content, we investigated the surface morphology of the P3HT/SPFGraphene composite films with different SPFGraphene contents (2.5 wt %, 5 wt %, 10 wt %, 15 wt %) by the use of scanning electron microscopy (SEM), as shown in Figure 8. In the P3HT/SPFGraphene composite film containing 2.5 wt % SPFGraphene (Figure 8a), only a few graphene sheets can be seen embedded in the P3HT matrix and separated from each other. It can be deduced that, in the photovoltaic device based on this composite film, the graphene content is too low to form enough D/A interfaces for the charge generation. The graphene sheets cannot form continuous pathways in the P3HT matrix for the effective electron transport. Therefore, the performance of the photovoltaic device made with this SPFGraphene content is very low. In the composite film with 5 wt % SPFGraphene (Figure 8b), there are more graphene sheets than in the film with 2.5 wt % SPFGraphene. Therefore, more-effective charge generation and transport will be obtained in the film with 5 wt % of SPFGraphene compared with that in the film with 2.5 wt % SPFGraphene. Whereas the graphene content is still not enough to form a continuous network structure, so the charge transport is still not efficient in the composite film. Figure 8c shows the composite film with 10 wt % SPFGraphene. The graphene sheets are well dispersed and well wetted in this composite film and form abundant D/A interfaces for charge generation; they connect with one another and form an interpenetrating network. Compared with the composite films having lower SPFGrapene contents (2.5 and 5 wt %), it is not difficult to understand that photovoltaic devices based on this composite active layer have much-better cell performance. Figure 8d shows the film morphology of the composite with a SPFGraphene content of 15 wt %. In this composite film, there are so many graphene sheets that they aggregate to form great agglomerates. The surface of the composite film was no longer flat upon the aggregation of the graphene sheet. In view of the strong aggregation of SPFGraphene in P3HT matrix, it is understandable that the performance of photovoltaic devices based on this active layer was worse than that for those with a SPFGraphene content of 10 wt %. By comparing the UV-vis/NIR absorption properties of the P3HT and P3HT/SPFGraphene mixture, it can be seen that the light harvesting of the P3HT/SPFGraphene-based photovoltaic device mainly comes from the P3HT; this indicates that the active layer containing much-more P3HT exhibits a better light-absorbing ability. Therefore, with a lower loading of SPFGraphene in the P3HT matrix when the optimized D/A interface and continuous charge-transport pathway are formed, a higher solar-harvesting efficiency will be obtained. Therefore, the relatively low acceptor content (~10%) at which the optimized power-conversion efficiency can be obtained indicates the great superiority of the graphene used as the electron acceptor material.

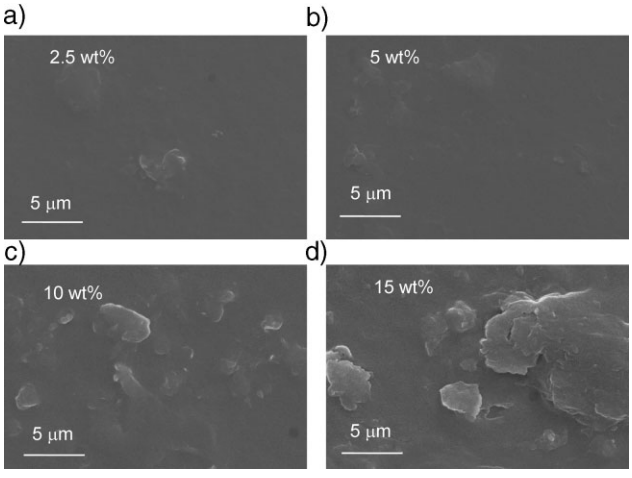

Figure 8. SEM pictures of P3HT/SPFGraphene composite films on glass with different SPFGraphene contents (2.5 wt %, 5 wt %, 10 wt %, and 15 wt %). The films were made by spin-coating the solutions of P3HT/SPFGraphene (P3HT: 15mg mL^{-1}, SPFGraphene contents of 2.5 wt %, 5 wt %, 10 wt %, and 15 wt %) at 2000 rpm.

From Figure 8, it can be seen that the graphene sheets tend to take a conformation parallel to the film plane: they prefer to ''lie'' flat rather than ''stand'' in the P3HT matrix. Such a configuration of graphene sheets avoids short-circuits of the photovoltaic cells, which has been proved to be a problem in CNT-based photovoltaic devices.[90] While this configuration of the graphene sheet is unfavorable for charge transfer in the photocurrent generation because the most-convenient pathway for hole and electron transfer in the active layer is vertical to the film plain, it will take a minimum time and distance for the charge to be transported to and collected by the relevant electrodes. Although wrinkling of the graphene sheets and their interconnection can also form pathways for electron transfer to the electrodes, the stacking configuration of the graphene sheets in the P3HT matrix is inefficient for charge transfer, as can be revealed by the relatively low *FF* values of the devices, even with annealing treatment. Therefore, there is much room for improving the cell efficiency by fine control of the composite morphology.

3. Conclusions

In conclusion, an organic solution-processable graphene (SPFGraphene) with a size dimension of several hundreds of nanometers was used as the acceptor material in organic BHJ photovoltaic devices with P3HT as the electron-donor material. The functionalized graphene can be well dispersed in P3HT to form a donor/acceptor structure with 10 wt % doping. Adding SPFGraphene into P3HT induces great quenching of the photoluminescence of the P3HT, indicating strong electron/energy transfer from the P3HT to the graphene. The interaction between the graphene and the P3HT makes this composite work well as the active layer in the BHJ photovoltaic devices. In the photovoltaic devices with an ITO/PEDOT:PSS/P3HT:graphene/LiF/Al structure, a power-conversion efficiency of 1.1% was

obtained under simulated AM1.5G conditions by use of xenon-light illumination at 100 mW cm^{-2} for the device with a graphene content of 10 wt %. With the increase in the graphene content, the device efficiency increases first and then decreases, the device containing only 10 wt % of graphene shows the best performance. The film morphology analysis using SEM shows that the film with a graphene content of 10 wt % shows the best interpenetrating network, while the graphene sheets below a 10 wt % content cannot interconnect with one another and a much-higher graphene content leads to strong aggregation. Annealing the device at 160 °C for 10 min improves the device efficiency to 1.1%, with an open-circuit voltage (V_{oc}) of 0.72 V, a short-circuit current density (J_{sc}) of 4.0 mA cm^{-2}, and a fill factor (*FF*) of 0.38, whereas annealing the device at overgenerous conditions such as at 210 °C for 10 min results in a decrease in the device efficiency (0.57%). The fill factor of the devices is not high, even after the annealing treatment, which may be due to the parallel configuration of the graphene sheets to the film plane, as evidenced by transmission electron microscopy (TEM). Although this configuration of the graphene sheets avoids a short circuit, it is not favorable for charge transfer. Therefore, there is much room for the improvement in the device performance, including fine control of the graphene size, annealing conditions, film morphology, and so on.

4. Experimental

Preparation of Graphene Oxide: Graphene oxide was prepared using a modified Hummers method from flake graphite (average particle diameter of 4 μm, 99.95% purity, Qingdao Tianhe Graphite Co., Ltd.)[1]. Briefly, graphite (5 g) and $NaNO_3$ (A.R., 3.75 g) were placed in a flask. Then, H_2SO_4 (A.R., 375 mL) was added with stirring in an ice-water bath. $KMnO_4$ (A.R., 22.5 g) was slowly added over about 1 h. Cooling was completed in 2 h, and the mixture was allowed to stand for five days at room temperature with vigorous stirring. During the five days, the mixture changed from green to dark brown to brick brown. The liquid obtained was added to H_2SO_4 aqueous solution (700 mL, 5 wt %) over about 1 h with stirring and the temperature was kept at 98 °C; the resultant mixture was further stirred for 2 h. Then the temperature was cooled down to 60 °C and H_2O_2 (15 mL, 30 wt % aqueous solution) was added to the above liquid and the mixture was stirred for 2 h at room temperature.

In order to remove ions of oxidant origin, especially manganese ions, the resultant liquid was purified by repeating the following procedure cycle at least 15 times: centrifugation, removal of the supernatant liquid, addition of mixed aqueous solution (2 L) of H_2SO_4 (3 wt %)/H_2O_2 (0.5 wt %) and dispersion using vigorous stirring and bath ultrasonication for 30 min at a power of 140 W. Then the procedure was cycled 3 times using aqueous HCl solution (3 wt %) and for twice using H_2O. The resultant solution was transferred to acetone to remove the remaining acid. Then, through a drying process, the graphene oxide was obtained.

Isocyanate Functionalization of Graphene Oxide: The functionalization process of the graphene oxide was as follows: dried graphite oxide (200 mg) was suspended in anhydrous *N,N*-dimethylformamide (DMF) (20 mL), and treated with phenyl isocyanate (A.R., 20 g) for 1 week. After a work-up procedure to remove the impurities, the isocyanate-treated graphene oxide was obtained. The reaction mixture was added drop-wise into DCB (25 mL) and centrifuged at 1 000 rpm for 10 min. The upper solution was dropped into $CHCl_3$ (50 mL) and centrifuged at 11 000 rpm to collect the deposit at the bottom. This procedure was repeated twice to get the purified functionalized graphene with a yield of 70%.

Fabrication of the Photovoltaic Devices: Poly(3-hexylthiophene) was purchased from Aldrich Chemical Co. The materials were synthesized by the Rieke method. The head-to-tail (HT) regioregularity reported by the company was >98.5%. The number-average molecular weight of P3HT was reported as $M_n = 60\,000$–$70\,000$ with a PDI of ~1.8. The devices were prepared from a P3HT/graphene solution in 1,2-dichlorobenzene (P3HT content: 15 mg mL^{-1}, graphene contents: 0 to 15 wt %). Poly(3,4-ethylenedioxythiophene):poly(styrenesulfonate) (PEDOT:PSS) (Baytron P, Bayer Germany) was then spin-coated (4000 rpm, ~40 nm thickness) on the top of ITO-coated glass. The active layer was prepared by spin-coating (2000 rpm, 9 s) on the above modified ITO glass using a solution of P3HT (15 mg mL^{-1})/graphene (0 wt % to 15 wt %) in DCB. The active-layer thickness was measured as ~100 nm by use of a profilometer (Ambios, XP-2TM). The annealing was carried out at 160 °C and 210 °C for 10 and 20 min in a glove box. Then, lithium fluoride (LiF, ~1 nm) and the Al electrode (70 nm) were deposited onto the blend film by thermal evaporation at a vacuum of ca. 5×10^{-6} mbar. Eight polymer solar-cell devices were fabricated in one cut ITO glass, and the effective area of every cell was ~8 mm^2. All of the current–voltage (*J–V*) characteristics of the photovoltaic devices were measured in air using a Keithley SMU 2400 unit. A xenon lamp with a filter (broadpasss GRB-3, Beijing Changtuo Scientific Limited Company) to simulate AM1.5G conditions was used as the excitation source white-light illumination from the ITO side, with a power of 100 mW cm^{-2}. The light-source illumination intensity was measured using a calibrated broadband optical power meter (F2-A, wavelength range 400-1000 nm, Photoelectric Instrument Co, Beijing Normal University, China). All of the fabrication and measurements were conducted in air at room temperature. The calculation of the power-conversion efficiency, η, was performed using Equation (1):

$$\eta = \frac{V_{OC} J_{SC} FF}{P_{in}} \quad (1)$$

In Equation (1), V_{oc}, J_{sc}, *FF*, and P_{in} are the open circuit voltage, the short circuit current density, the fill factor and the incident light power, respectively. The fill factor (*FF*) was determined according to $FF = (V_m \cdot J_m)/(V_{oc} \cdot J_{sc})$, where V_m and J_m are the voltage and the current density at the maximum-power point of the *J–V* curve in the fourth quadrant.

AFM, SEM, UV-Vis-NIR Spectroscopy, PL Spectroscopy, TGA-DSC, and Elemental Analysis: For AFM measurements, the graphene oxide sample was prepared by spin-coating (2000 rpm, 30 s) a graphene oxide solution (0.2 mg mL^{-1}) in H_2O on a mica surface. AFM studies were performed using a Digital Instruments Dimension 3100 in the tapping mode. For SEM measurements, composite films of P3HT/graphene were prepared by spin-coating (2000 rpm, 9 s) on the above modified ITO glass using the solution of P3HT (15 mg mL^{-1}) and graphene (2.5 wt % to 15 wt %) in DCB. The sample films were gold-coated and the images were taken on a Hitachi S-3500 N scanning electron microscope. For the UV-vis-NIR spectroscopy and the photoluminescence measurements, a P3HT/SPFGraphene (P3HT: 1 mg mL^{-1}, SPFGraphene content: 10 wt %) solution in DCB, as well as a reference solution of P3HT (1 mg mL^{-1}) in DCB were used. UV-vis-NIR spectra were obtained with a JASCO V-570 spectrometer. Photoluminescence measurements were carried out using a Fluoro Max-P spectrometer (Jobin–Yvon) with excitation at 422 nm. Thermogravimetric analyses (TGA) and differential scanning calorimetry (DSC) analyses were performed using a TGA/DSC STA904 at a heating rate of 5 °C min^{-1} under a nitrogen flow. Elemental analysis was carried using a Yanaca CDRDER MT-3 instrument.

Acknowledgements

The authors gratefully acknowledge the financial support from NSF (60876046, 60676051, 20644004, 07JCYBJC03000) of China, Tianjin Natural Science Foundation (06TXTJJC14603), MoST (2006CB0N0702), MoE (20040055020).

Received: July 9, 2008
Published online: February 13, 2009

[1] A. C. Mayer, S. R. Scully, B. E. Hardin, M. W. Rower, M. D. McGehee, *Mater. Today* **2007**, *10*, 28.
[2] B. C. Thompson, J. M. J. Fréchet, *Angew. Chem. Int. Ed.* **2008**, *47*, 58.
[3] C. J. Brabec, N. S. Sariciftci, J. C. Hummelen, *Adv. Funct. Mater.* **2001**, *11*, 15.
[4] C. J. Brabec, S. N. Sariciftci, *Monatshefte Chem. - Chem Monthly* **2001**, *132*, 421.
[5] A. J. Moulé, K. Meerholz, *Adv. Mater.* **2008**, *20*, 240.
[6] J. Peet, J. Y. Kim, N. E. Coates, W. L. Ma, D. Moses, A. J. Heeger, G. C. Bazan, *Nat. Mater.* **2007**, *6*, 497.
[7] G. Li, V. Shrotriya, J. S. Huang, Y. Yao, T. Moriarty, K. Emery, Y. Yang, *Nat. Mater.* **2005**, *4*, 864.
[8] W. L. Ma, C. Y. Yang, X. Gong, K. Lee, A. J. Heeger, *Adv. Funct. Mater.* **2005**, *15*, 1617.
[9] K. Kim, J. Liu, M. A. G. Namboothiry, D. L. Carroll, *Appl. Phys. Lett.* **2007**, *90*, 163511.
[10] J. Y. Kim, K. Lee, N. E. Coates, D. Moses, T. Q. Nguyen, M. Dante, A. J. Heeger, *Science* **2007**, *317*, 222.
[11] C. J. Brabec, N. S. Sariciftci, J. C. Hummelen, *Adv. Funct. Mater.* **2001**, *11*, 15.
[12] S. R. Forrest, *MRS Bull.* **2005**, *30*, 28.
[13] J. Xue, B. P. Rand, S. Uchida, S. R. Forrest, *Adv. Mater.* **2005**, *17*, 66.
[14] F. Padinger, R. S. Rittberger, N. S. Sariciftci, *Adv. Funct. Mater.* **2003**, *13*, 85.
[15] C. W. Tang, *Appl. Phys. Lett.* **1986**, *48*, 183.
[16] G. Yu, J. Gao, J. C. Hummelen, F. Wudl, A. J. Heeger, *Science* **1995**, *270*, 1789.
[17] J. M. Halls, C. A. Walsh, N. C. Greenham, E. A. Marseglia, R. H. Friend, S. C. Moratti, A. B. Holmes, *Nature* **1995**, *376*, 498.
[18] S. R. Scully, M. D. McGehee, *J. Appl. Phys.* **2006**, *100*, 034907.
[19] D. E. Markov, J. C. Hummelen, P. W. M. Blom, A. B. Sieval, *Phys. Rev. B: Condens. Matter* **2005**, *72*, 045216.
[20] P. Peumans, A. Yakimov, S. R. Forrest, *J. Appl. Phys.* **2003**, *93*, 3693.
[21] D. Veldman, T. Offermans, J. Sweelssen, M. M. Koetse, S. C. J. Meskers, R. A. J. Janssen, *Thin Solid Films* **2006**, *511*, 333.
[22] M. M. Alam, S. A. Jenekhe, *Chem. Mater.* **2004**, *16*, 4647.
[23] T. Kietzke, H. H. Horhold, D. Neher, *Chem. Mater.* **2005**, *17*, 6532.
[24] M. M. Koetse, J. Sweelssen, K. T. Hoekerd, H. F. M. Schoo, S. C. Veenstra, J. M. Kroon, X. Yang, J. Loos, *Appl. Phys. Lett.* **2006**, *88*, 083504.
[25] J. J. Dittmer, K. Petritsch, E. A. Marseglia, R. H. Friend, H. Rost, A. B. Holmes, *Synth. Met.* **1999**, *102*, 879.
[26] J. J. Dittmer, R. Lazzaroni, P. Leclere, P. Moretti, M. Granstrom, K. Petritsch, E. A. Marseglia, R. H. Friend, J. L. Bredas, H. Rost, A. B. Holmes, *Sol. Energy Mater. Sol. Cells* **2000**, *61*, 53.
[27] J. J. Dittmer, E. A. Marseglia, R. H. Friend, *Adv. Mater.* **2000**, *12*, 1270.
[28] L. H. Nguyen, H. Hoppe, T. Erb, S. Gunes, G. Gobsch, N. S. Sariciftci, *Adv. Funct. Mater.* **2007**, *17*, 1071.
[29] F. Yang, M. Shtein, S. R. Forrest, *Nat. Mater.* **2005**, *4*, 37.
[30] P. Peumans, S. Uchida, S. R. Forrest, *Nature* **2003**, *425*, 158.
[31] L. Schmidt-Mende, A. Fechtenkotter, K. Mullen, E. Moons, R. H. Friend, J. D. MacKenzie, *Science* **2001**, *293*, 1119.
[32] H. Bässler, *Mol. Cryst. Liq. Cryst. Sci. A* **1994**, *252*, 11.
[33] W. U. Huynh, J. J. Dittmer, A. Paul, *Science* **2002**, *295*, 2425.
[34] E. Kymakis, E. Koudoumas, I. Franghiadakis, G. A. J. Amaratunga, *J. Phys. D: Appl. Phys.* **2006**, *39*, 1058.
[35] H. Ago, K. Petritsch, M. S. P. Shaffer, A. H. Windle, R. H. Friend, *Adv. Mater.* **1999**, *11*, 1281.
[36] J. X. Geng, T. Y. Zeng, *J. Am. Chem. Soc.* **2006**, *128*, 16827.
[37] B. J. Landi, R. P. Ruffaelle, S. L. Castro, S. G. Bailey, *Prog. Photovoltaics: Res. Appl.* **2005**, *13*, 165.
[38] E. Kymakis, G. A. J. Amaratunga, *Appl. Phys. Lett.* **2002**, *80*, 112.
[39] E. Kymakis, I. Alexandrou, G. A. J. Amaratunga, *J. Appl. Phys.* **2003**, *93*, 1764.
[40] J. Boucle, P. Ravirajan, J. Nelson, *J. Mater. Chem.* **2007**, *17*, 3141.
[41] B. Sun, H. J. Snaith, A. S. Dhoot, S. Westenhoff, N. C. Greenham, *J. Appl. Phys.* **2005**, *97*, 014914.
[42] P. Wang, A. Abrusci, H. M. P. Wong, M. Svensson, M. R. Andersson, N. C. Greenham, *Nano Lett.* **2006**, *6*, 1789.
[43] W. J. E. Beek, M. M. Wienk, R. A. J. Janssen, *Adv. Mater.* **2004**, *16*, 1009.
[44] B. Q. Sun, N. C. Greenham, *Phys. Chem. Chem. Phys.* **2006**, *8*, 3557.
[45] E. Palacios-Lidon, B. Perez-Garcia, J. Abellan, C. Miguel, A. Urbina, J. Colchero, *Adv. Funct. Mater.* **2006**, *16*, 1975.
[46] K. S. Novoselov, A. K. Geim, S. V. Morozov, D. Jiang, Y. Zhang, S. V. Dubonos, I. V. Grigorieva, A. A. Firsov, *Science* **2004**, *306*, 666.
[47] K. S. Nonoselov, E. McCann, S. V. Morozov, V. I. Fal'ko, M. I. Katsnelson, U. Zeitler, D. Jiang, F. Schedin, A. K. Geim, *Nature Phys.* **2006**, *2*, 177.
[48] K. S. Novoselov, Z. Jiang, Y. Zhang, S. V. Morozov, H. L. Stormer, U. Zeitler, J. C. Maan, G. S. Boebinger, P. Kim, A. K. Geim, *Science* **2007**, *315*, 1379.
[49] K. S. Novoselov, A. K. Geim, S. V. Morozov, D. Jiang, M. I. Katsnelson, I. V. Grigorieva, S. V. Dubonos, A. A. Firsov, *Nature* **2005**, *438*, 197.
[50] V. P. Gusynin, S. G. Sharapov, *Phys. Rev. Lett.* **2005**, *95*, 146801.
[51] Y. B. Zhang, Y. W. Tan, H. L. Stormer, P. Kim, *Nature* **2005**, *438*, 201.
[52] S. Y. Zhou, G. H. Gweon, J. Graf, A. V. Fedorov, C. D. Spataru, R. D. Diehl, Y. Kopelevich, D. H. Lee, S. G. Louie, A. Lanzara, *Nature Phys.* **2006**, *2*, 595.
[53] Y. Kim, S. Cook, S. M. Tuladhar, S. A. Choulis, J. Nelson, J. R. Durrant, D. D. C. Bradley, M. Giles, I. Mcculloch, C. S. Ha, M. Ree, *Nat. Mater.* **2006**, *5*, 197.
[54] S. Gilje, S. Han, M. Wang, K. L. Wang, R. B. Kaner, *Nano Lett.* **2007**, *7*, 3394.
[55] D. Gunlycke, D. A. Areshkin, C. T. White, *Appl. Phys. Lett.* **2007**, *90*, 142104.
[56] B. Obradovic, R. Kotlyar, F. Heinz, P. Matagne, T. Rakshit, M. D. Giles, M. A. Stettler, D. E. Nikonov, *Appl. Phys. Lett.* **2006**, *88*, 142102.
[57] Y. Ouyang, Y. Yoon, J. K. Fodor, J. Guo, *Appl. Phys. Lett.* **2006**, *89*, 203107.
[58] M. Y. Han, B. Ozyilmaz, Y. Zhang, P. Kim, *Phys. Rev. Lett.* **2007**, *98*, 206805-1.
[59] J. S. Bunch, A. M. van der Zande, S. S. Verbridge, I. W. Frank, D. M. Tanenbaum, J. M. Parpia, H. G. Craighead, . P. L. McEuen, *Science* **2007**, *315*, 490.
[60] B. Trauzettel, D. V. Bulaev, D. Loss, G. Burkard, *Nature Phys.* **2007**, *3*, 192.
[61] S. Watcharotone, D. A. Dikin, S. Stankovich, R. Piner, I. Jung, G. H. B. Dommett, G. Evmenenko, S. E. Wu, S. F. Chen, C. P. Liu, S. T. Nguyen, R. S. Ruoff, *Nano Lett.* **2007**, *7*, 1888.
[62] X. Wang, L. Zhi, K. Mullen, *Nano Lett.* **2008**, *8*, 323.
[63] H. Becerril, J. Mao, Z. Liu, R. M. Stoltenberg, Z. Bao, Y. Chen, *ACS Nano* **2008**, *2*, 463.
[64] Q. Liu, Z. Liu, X. Zhang, N. Zhang, L. Yang, S. Yin, Y. Chen, *Appl. Phys. Lett.* **2008**, *92*, 223303.
[65] Z. Liu, Q. Liu, Y. Huang, Y. Ma, S. Yin, X. Zhang, W. Sun, Y. Chen, *Adv. Mater.* **2008**, *20*, 3924.
[66] T. A. Land, T. Michely, R. J. Behm, J. C. Hemminger, G. Comsa, *Surf. Sci.* **1992**, *264*, 261.
[67] A. Nagashima, K. Nuka, H. Itoh, T. Ichinokawa, C. Oshima, S. Otani, *Surf. Sci.* **1993**, *291*, 93.
[68] A. K. Geim, K. S. Novoselov, *Nat. Mater.* **2007**, *6*, 183.
[69] S. Stankovich, D. A. Dikin, G. H. B. Dommett, K. M. Kohlhaas, E. J. Zimney, E. A. Stach, R. D. Piner, S. B. T. Nguyen, R. S. Ruoff, *Nature* **2006**, *442*, 282.
[70] S. Stankovich, R. D. Piner, X. Q. Chen, N. Q. Wu, S. T. Nguyen, R. S. Ruoff, *J. Mater. Chem.* **2006**, *16*, 155.
[71] W. S. Hummers, R. E. Offeman, *J. Am. Chem. Soc.* **1958**, *80*, 1339.
[72] H. He, J. Klinowski, M. Forster, A. Lerf, *Chem. Phys. Lett.* **1998**, *287*, 53.
[73] M. Hirata, T. Gotou, S. Horiuchi, M. Fujiwara, M. Ohba, *Carbon* **2004**, *42*, 2929.
[74] S. Niyogi, E. Bekyarova, M. E. Itkis, J. L. McWilliams, M. A. Hamon, R. C. Haddon, *J. Am. Chem. Soc.* **2006**, *128*, 7720.
[75] S. Stankovich, D. A. Dikin, R. D. Piner, K. A. Kohlhaas, A. Kleinhammes, Y. Jia, Y. Wu, S. T. Nguyen, R. S. Ruoff, *Carbon* **2007**, *45*, 1558.

[76] C. Gomez-Navarro, R. T. Weitz, A. M. Bittner, M. Scolari, A. Mews, M. Burghard, K. Kern, *Nano Lett.* **2007**, *7*, 3499.
[77] S. Stankovich, R. D. Piner, S. T. Nguyen, R. S. Ruoff, *Carbon* **2006**, *44*, 3342.
[78] S. Berson, R. de Bettignies, S. Bailly, S. Guillerez, B. Jousselme, *Adv. Funct. Mater.* **2007**, *17*, 3363.
[79] Y. H. Kim, D. Spiegel, S. Hotta, A. J. Heeger, *Phys. Rev. B: Condens. Matter* **1988**, *38*, 5490.
[80] B. Xu, S. Holdcroft, *Macromolecules* **1993**, *26*, 4457.
[81] N. S. Sariciftci, L. Smilowitz, A. J. Heeger, F. Wudl, *Science* **1992**, *258*, 1474.
[82] M. Al-Ibrahim, H.-K. Roth, U. Zhokhavets, G. Gobsch, S. Sensfuss, *Sol. Energy Mater. Sol. Cells* **2005**, *85*, 13.
[83] C. J. Brabec, A. Cravino, D. Meissner, N. S. Sariciftci, T. Fromherz, M. T. Rispens, L. Sanchez, J. C. Hummelen, *Adv. Funct. Mater.* **2001**, *11*, 374.
[84] I. D. Parker, *J. Appl. Phys.* **1994**, *75*, 1656.
[85] M. C. Scharber, D. Wuhlbacher, M. Koppe, P. Denk, C. Waldauf, A. J. Heeger, C. L. Brabec, *Adv. Mater.* **2006**, *18*, 789.
[86] R. Czerw, B. Foley, D. Tekleab, A. Rubio, P. M. Ajayan, D. L. Carroll, *Phys. Rev. B: Condens. Matter* **2002**, *66*, 033408.
[87] J. W. G. Wildoer, L. C. Venema, A. G. Rinzler, R. E. Smalley, C. Dekker, *Nature* **1998**, *391*, 59.
[88] P. Andersson, N. D. Robinson, M. Berggren, *Synth. Met.* **2005**, *150*, 217.
[89] M. M. Mandoc, L. J. A. Koster, P. W. M. Blom, *Appl. Phys. Lett.* **2007**, *90*, 133504.
[90] D. B. Romero, M. Carrard, W. DeHeer, L. Zuppiroli, *Adv. Mater.* **1996**, *8*, 899.